ISSN: 2476-230X

Research Article

Cardiology: Open Access

Temporal Changes in Key Signal Transduction Pathways Mediating Muscle Protein Synthesis with Adaptive and Maladaptive Right Ventricular Hypertrophy in Pulmonary Arterial Hypertension

Ryan C Middleton[1,3], Mario Fournier[1], Russell G Rogers[1], Brandon S Grimes[2], Xuan Xu[2], Michael I Lewis[1,2*]

[1]Smidt Heart Institute, Cedars-Sinai Medical Center, Los Angeles, CA, USA

[2]Division of Pulmonary/Critical Care Medicine, Cedars-Sinai Medical Center, Los Angeles, CA, USA

[3]Jacobs School of Engineering, University of California, San Diego, CA, USA

[*]Corresponding Author
Michael I Lewis, Smidt Heart Institute and Division of Pulmonary/Critical Care Medicine, Cedars-Sinai Medical Center, Los Angeles, CA, USA.

Submitted: 21 Dec 2022; **Accepted:** 28 Dec 2022; **Published:** 05 Jan 2023

Citation: Middleton, R. C., Fournier, M., Rogers, R. G., Grimes, B. S., Xu, X., & Lewis, M. I. (2023). Temporal Changes in Key Signal Transduction Pathways Mediating Muscle Protein Synthesis with Adaptive and Maladaptive Right Ventricular Hypertrophy in Pulmonary Arterial Hypertension. *Cardio Open*, 8(1), 01-14.

Abstract

Pulmonary Arterial Hypertension (PAH) is a progressive disease characterized by occlusive remodeling of pulmonary arteries < 500 micron and increased pulmonary vascular resistance. With the onset of PAH, the right ventricle (RV) of the heart adapts to the increased afterload pressure by undergoing adaptive hypertrophic remodeling to maintain adequate blood flow. However, for unknown reasons, maladaptive influences ensue, resulting in impaired RV function with progressive decompensation and right heart failure. Using a rodent model of PAH, key signaling pathways mediating cardiac muscle protein synthesis in the RV were evaluated during both the adaptive hypertrophy phase, with preserved right heart function, and the decompensated maladaptive phase, in which right heart failure (RHF) was present.

Analysis of protein and gene expression changes in PAH animals identified three key signaling pathways involved in the shift toward maladaptive right heart failure: i) PI3K/Akt/mTOR; ii) GSK-3; iii) MAPK/ERK, as well as IGF-1 regulation. During adaptive hypertrophy, significant increments of phosphorylated proteins in the three signaling pathways were observed with increases in RV fibrosis and decreased capillarity found. In the maladaptive phase, mTORC1 and its downstream effector p-70^{S6K} were significantly activated, contributing to the decreased LC3-I/II ratio, a marker of autophagy inhibition together with further significant RV muscle fibrosis and greater capillary rarefaction.

We propose that autophagy inhibition in conjunction with other maladaptive processes reported in the decompensated RV muscle contributes to the genesis of overt RHF in PAH, and that a continuum of changes characterizes the adaptive and maladaptive phases in the RV muscle

Keywords: Pulmonary Arterial Hypertension (PAH), Right Heart Failure (RHF), Autophagy, Cell Signaling, Monocrotaline

Introduction

Pulmonary arterial hypertension (PAH) is a progressive condition for which there is no cure. Even with substantial pharmacologic advances in the modern treatment era, survival remains unacceptably poor [1-3]. PAH is characterized by occlusive remodeling of pulmonary arteries < 500 micron and increased pulmonary vascular resistance. With the onset of PAH, the right ventricle (RV) adapts to the increased afterload presented to it by adaptive hypertrophy to maintain adequate blood flow. This is driven by signaling events that promote enhanced muscle protein synthesis and physiologic growth. However, for unknown reasons, maladaptive influences ensue, resulting in impaired RV function with progressive decompensation and failure [4]. Indeed, RV function is the major factor determining survival of patients with PAH [5-8].

We and others have reported that several signaling pathways involved in muscle protein synthesis are important mediators of adaptive cardiac and skeletal muscle hypertrophy. This includes the phosphatidylinositol 3-kinase (PI3K)/Akt/mammalian target of rapamycin (mTOR) pathway, as a major regulator of cardiac and skeletal muscle protein synthesis and hypertrophy, with significant depression in the diaphragm muscle in atrophic states [9-15]. Another signaling pathway mediating enhanced cardiac muscle protein synthesis and growth, is the glycogen synthase kinase-3 (GSK-3) pathway which plays a key role in the inte-

gration of hypertrophic signaling in the heart, involving both α and β isoforms [16,17]. Lastly, the mitogen-activated protein kinases (MAPK)/extracellular signal-regulated kinases (ERK) 1/2 pathways also exhibit significant influences in promoting cardio myocyte hypertrophy [15,18-20]. We postulate that these three signaling pathways would be key in mediating adaptive changes in the RV muscle exposed to a slow progressive rise in RV afterload facing the RV as PAH develops.

In this study, the temporal changes in the signaling of these three pathways were measured in the RV muscle as the RV progresses from a healthy state to adaptive hypertrophy and then to maladaptive hypertrophy in an animal model of PAH. In addition, insulin like growth factor-1 (IGF-1) was evaluated in adaptive and maladaptive RVs, as this growth factor has been shown to both impact upon these three pathways and has been implicated in reports of physiologic cardiac hypertrophy as well as signature of RV failure [10,21-24]. Furthermore, signaling proteins associated with autophagy were assessed in the decompensated maladapted RV muscle of rats with established right ventricular dysfunction and failure. PAH progression was established by echocardiographic parameters of impaired RV systolic function along with confirmatory changes at the cellular level, which included changes in RV wall fibrosis and capillarity.

In the monocrotaline (MCT) rat model of PAH, observations in both the adapted and maladapted states describe several directions of change in the RV muscle that were unanticipated based on skeletal muscle data and provide robust data and important questions for future research endeavors in fully understanding RV physiologic and pathologic changes that occur in the RV with progressive PAH [15].

Methods

Animal Care

Adult male Sprague-Dawley rats (initial body weight ~225g; n=52) were divided into 2 major groups, namely control (CTL) and PAH. The CTL rats were injected subcutaneously with saline, while the PAH animals received a single subcutaneous injection of MCT (Sigma, St. Louis, MO) at a dose of 60 mg/kg body weight, dissolved in 0.5mL saline. All animals were provided with food (Purina rat chow) and water ad libitum. Animals were individually housed with a dark: light cycle of 12 hours each and with the ambient temperature maintained at 22ºC. Terminal experiments were performed at days 7, 14, 24 and 28 (adapted cohort) and at 42 days (maladapted cohort, based on echocardiography).

Echocardiography

Transthoracic two-dimensional, M-mode echocardiography and pulsed-wave Doppler imaging were performed on anesthetized (isoflurane) rats (Vevo 770 Micro-Ultrasound imaging system; Visual Sonics: Toronto, Canada). RV systolic function was determined by tricuspid annular plane systolic excursion (TAPSE), recorded in M-mode. Doppler of pulmonary outflow measured pulmonary artery flow velocity time (PAVTI). To obtain stroke volume (SV), the cross-sectional area of the pulmonary artery was multiplied by PAVTI, and estimated cardiac output (CO) was derived by multiplying SV by heart rate. Serial studies were performed before and post MCT administration.

Histological Studies

Fibrosis: To assess fibrosis, cryosections of RV free wall from 5 adapted, 5 maladapted and 3 CTL rats were stained with Picrosirius Red as described [25,26]. Sections were imaged by bright field microscopy and analysis was performed using ImageJ (Fiji), by measuring pixel density within the green channel throughout the entire RV free wall [27,28]. One section was analyzed for each animal and normalized to the total area of the RV free wall. Results are presented as percent fibrosis.

Vessel counts: To assess vascularity in CTL, adapted and maladapted RV free wall from PAH animals, 10μm tissue sections were stained with anti-rat smooth muscle actin primary antibody (1:100, Sigma) and FITC-conjugated goat anti-rat secondary antibody (1:400, Abcam), and TRITC conjugated isolectin IB4 (Thermo). The stained tissue sections were imaged by confocal microscopy (Leica) and analyzed using ImageJ (Fiji). 10 cryosections were analyzed per animal.

Muscle Proteins

Protein Extraction: RV muscle segments were rapidly frozen in liquid nitrogen and stored at -80°C until analysis. Sample protein was extracted in a 1:10 ratio of cold RIPA buffer (Cell Signaling Technologies, Beverly, MA), with protease and phosphatase inhibitors (Roche, South San Francisco, CA) added, according to manufacturer's protocol. For mTOR analysis samples, 0.4% CHAPS was also added to the lysis buffer. Homogenization was performed with a Polytron homogenizer (Kinematic, Bohemia, and NY) and tissue lysates were incubated on ice for 4 hours and then were centrifuged at 13,200 RPM. The supernatant was aliquoted in micro centrifuge tubes. Protein concentration was determined using a commercial protein assay kit (Bio-Rad, Hercules, CA) and measured with a spectrophotometer (Smart Spec™ 3000, Bio-Rad).

Immunoprecipitation: For mTOR analysis only, protein lysates were precleared with normal IgG (Santa Cruz Biotechnology, Dallas, TX) and protein A/G Plus-agarose beads (Santa Cruz Biotechnology). The lysates were incubated with the primary antibody (mTOR or phosphorylated mTOR (Ser^{2448}); Cell Signaling Technology, Beverly, MA) overnight at 4°C. Protein A/G Plus-agarose beads were added to the immunocomplex, incubated for 4 hours at 4°C, and centrifuged. The immunocomplex pellet was washed, resuspended in sample buffer, heated at 70°C for 15 min and centrifuged. The supernatant was used to load gels for electrophoresis as described below.

SDS-PAGE and Western blotting: Electrophoresis of protein extracts was performed by SDS-PAGE. In brief, samples were heated at 70°C for 15 min and cooled prior to being used for electrophoresis. Protein extracts (40 μg per well) were loaded on NuPAGE 4-12% Bis-Tris gradient gels (Invitrogen, Grand Island, NY). For the analysis of 4E-BP1 (PHAS-I) samples, extracts were loaded on 12% Bis-Tris gels. Separated proteins were then electrophoretically transferred to nitrocellulose membranes (Bio-Rad). The membranes were treated with blocking buffer for 1 hour at room temperature. Blots were incubated with primary antibodies at 4°C overnight, washed and incubated with an

appropriate peroxidase-conjugated secondary antibody at room temperature for 1 hour. The blots were visualized following development with enhanced chemiluminescence (ECL) Western blotting detection reagents (GE Healthcare Life Sciences, Pittsburgh, PA), according to manufacturers' protocol. Blots were re-used by exposing them to stripping buffer (Restore™, Thermo Scientific, and Rockford, IL) and re-probed with a different primary antibody to enable direct comparison of phosphorylated and non-phosphorylated states. Blots were exposed to X-ray film in a cassette, the films scanned, and identified bands analyzed by densitometry using ImageJ 1.43u (NIH). Western blot data from the experimental groups were expressed relative to measured mean values from the CTL group. All results are expressed as the ratio of phosphorylated protein/total protein.

Primary Antibodies: All primary antibodies were rabbit polyclonal antibodies obtained from Cell Signaling Technology, except for phosphospecific 4E-BP1 (Bethyl Laboratories, Montgomery, TX) and mouse monoclonal antibody for total GSK-3 (Santa Cruz Biotechnology). Blots were first incubated with the following anti-phosphopeptide (P) antibodies: P-Akt (Ser^{473}), P-$p70^{S6K}$ (Thr^{389}), P-GSK-3a/b ($Ser^{21/9}$), P-ERK1/2 (p44/p42) (Thr^{202}/Tyr^{204}), P-mTOR (Ser^{2448}), P-CDK2 (Thr^{160}), and P-4E-BP1 (PHAS-I). Stripped membranes were re-probed with antibodies recognizing total Akt, $p70^{S6K}$, GSK-3α/β, , ERK1/2 (p44/p42), mTOR, CDK2, 4E-BP1 as well as GAPDH, with the latter serving as a control for equal protein loading of samples. Blots to probe for non-phosphopeptide proteins were first incubated with p27, or LC3B antibodies.

IGF-1 protein measurement by ELISA: Determination of IGF-1 in the adaptive hypertrophy experiments was performed as previously described [29]. Briefly, frozen RV muscle segments were pulverized in liquid nitrogen. Protein was extracted twice on cold acetic acid (1M; 1 mg/10 µl) and supernatant stored at -80ºC overnight. Aliquots (100 µl) were lyophilized and stored frozen overnight. Protein pellets were resuspended in 40 µl H_2O and protein concentration determined as described above. Duplicate 10 µl protein samples were assayed using a commercial high sensitivity ELISA kit for rodent IGF-1 (AC-42F1) from Immunodiagnostic Systems, Inc. (IDS; Gaithersburg, MD) according to manufacturer's protocol.

Note, for the maladapted RV muscle IGF-1 assays a different kit was used, as the Immunodiagnostic Systems kit (AC-42F1) had been discontinued. Thus, for these experiments, we used a rat IGF-1 ELISA Kit (Catalog # 80573) from Crystal Chem (Elk Grove Village, IL). Results are expressed as ng/ mg protein.

RNA Extraction and Quantitative Polymerase Chain Reaction (qPCR)

Total RNA Extraction: Total RNA was extracted from RV muscle segments with RNeasy Mini Kit (Qiagen, Valencia, CA) according to manufacturer's protocol. RNA concentration was measured with a spectrophotometer (Nano Drop 1000; Thermo Scientific).

Oligonucleotides: The primers for IGF-1Ea and the reference gene succinate dehydrogenase A (SDH-A) were designed based on published rat cDNA sequences. Sequences of primers used for cDNA synthesis and RT-qPCR analysis, along with their accession number were the following: IGF-1Ea (NM_001082478): Forward 5'-GCTTGCTCACCTTTACCAGC-3', Reverse 5'-AAATGTACTTCCTTCTGAGTCT-3'; SDH-A (NM_130428): Forward 5'-CTCTTTTGGACCTTGTCGTCTTT-3', Reverse 5'-TCTCCAGCATTTGCCTTAATCGG-3'.

Real-time Quantitative PCR: RT-qPCR was performed in two steps. One ug of total RNA per sample was reverse transcribed with Superscript III using Oligo (dT)20 (Invitrogen) according to manufacturer's protocol. qPCR was performed in 10ul reactions using 2X Sybr Green Master Mix (ABi P/N 4309155), 50 nM gene specific primers, and 2ul of the reverse transcribed samples. Samples were analyzed in triplicates across the genes on the ABi Viia7. In order to compare the relative mRNA expression between control and experimental groups, the comparative threshold cycle (CT; the fractional cycle number at which the amount of amplified target reaches a fixed threshold) method was used.

Statistical Analysis

The distribution of all data was tested for normality and then statistical analysis was performed using ANOVA (Instat v. 3.06, Graph Pad, San Diego, CA) to compare differences between the independent groups in the adaptive state study. If a significant interaction was found, post hoc analysis (Student-Newman-Keuls test) was used to compare differences within independent groups. A Student t-test was used to compare differences between the groups in the maladaptive state study. A α level of 0.05 was used to compare differences in independent groups and to determine overall significance. Values are expressed as means ± SEM.

Results

Animal Physiology and RV Histology

To assess morphological and cell signaling changes in right ventricle cardiac tissue in a model of PAH, male Sprague-Dawley rats were treated with the pyrrolizidine alkaloid, Monocrotaline (MCT). Over the course of the disease, cardiac function was assessed, and cardiac tissues were collected and analyzed for gene expression changes as PAH progressed towards RHF. There are several physiological indicators of RV distress and failure that present during the progression of PAH, including changes in body weight, breathing rates and fluid retention in the abdominal cavity. Animals with PAH showed reduced body weight accumulation compared to healthy cohorts and will lose weight as the animals progressed towards RHF. During the RV adaptive phase of PAH, no difference in body weight was observed at day 7 post-MCT delivery between healthy controls (CTL) and PAH rats. At days 14, 24 and 28 days post-MCT, body weight gains were attenuated by 6, 8% and 14% respectively, for PAH animals compared to CTL ($P < 0.01$; Figure 1).

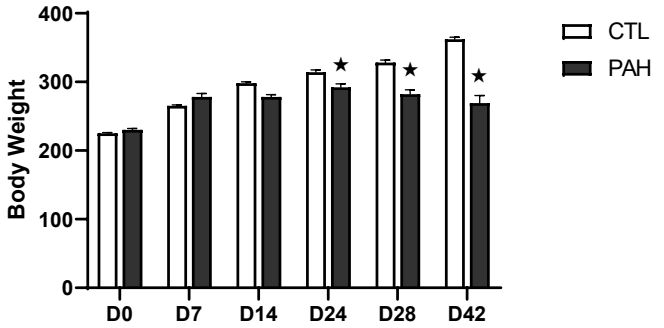

Figure 1: Body weights of control (CTL) and pulmonary arterial hypertension (PAH) animals at days 0, 7, 14, 24, and 28. Values are means ± SEM; ★significantly different from CTL animals.

At 42 days post-MCT at which time the animals exhibited overt RV dysfunction/failure, significant weight loss occurred, from peak weight achieved over time to weight at the time of terminal experiments (peak weight: 362 +/- 3 g; terminal weight: 269 +/- 11 g; $P < 0.01$). In addition, other observational signs suggestive of right heart failure were evident. This included a progressive listless state with obvious reduced mobility, poor grooming and ruffled fur and tachypnea with a pattern of increased work of breathing. Abdominal distension suggested the presence of ascites. Animals were sacrificed at this point, which was a joint decision by the investigators and veterinary staff. Post sacrifice, the presence of ascites +/- pleural effusions were confirmed.

TAPSE, a measure of RV systolic function by echocardiography, was assessed in MCT-treated rats and compared to CTL animals. No significant differences were observed between CTL rats and PAH animals from 7 to 28 days post MCT administration. (28 days, CTL: 2.9 +/- 0.7 mm; PAH: 2.8 +/- 0.14 mm). However, the mean value of TAPSE for the late-stage PAH cohort was significantly reduced compared to CTL and the group of adapted PAH animals (42 days, 1.73 +/- 0.144 mm; $P < 0.01$; Figure 2A). The estimated cardiac output (CO) for PAH rats at all time frames during the compensatory period were not significantly different from CTL values, and so the data was pooled for PAH animals (CTL: 124 +/- 8 ml/min; PAH: 100 +/- 4 ml/min). The values for CO of CTL rats were similar to those previously reported for male Sprague-Dawley rats of the same weight range [31]. For the maladapted cohort at 42 days post MCT, estimated value of CO was significantly reduced in these rats (72.6 +/- 5.1; SE; $P < 0.01$; Figure 2B).

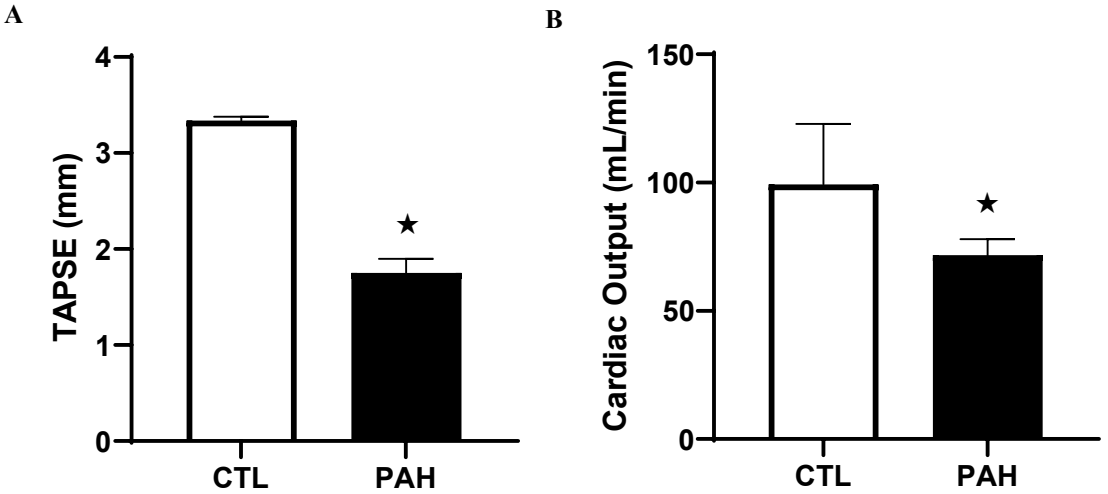

Figure 2A: Values of TAPSE in normal controls (CTL) compared to that in pulmonary arterial hypertension (PAH) rats complicated by right heart failure (RHF).
Figure 2B: Values of cardiac output (CO) in CTL animals compared to that in pulmonary arterial hypertension (PAH) rats complicated by RHF. ★Significantly different from CTL. Values are means ± SEM.

Histological assessment of fibrosis in coronal sections of RV free wall during the late adaptive RV hypertrophy stage (28 days post-MCT), indicated that the percentage area of the RV free wall occupied by fibrotic tissue increased more than 2-fold (9.07 +/- 1.70 %; SE) compared to CTL (3.97 +/- 1.20 %; $P < 0.05$; Figure 3A). Additionally, a further 1.8-fold increase in fibrosis (17.06 +/- 0.88 %; $P < 0.05$) was observed in the RV free wall of maladaptive hearts (42 days post-MCT) relative to the adapted RV cohort of PAH animals (Figure 3A). Changes in the RV free wall vascularity were assessed in CTL and PAH rats at both capillary and arteriolar levels. During late adaptive RV hypertrophy, the number of capillaries and arterioles in the RV free wall significantly decreased by 32% ($P < 0.05$) and 21% ($P < 0.05$), respectively, compared to CTL (Figure 3B&C). By contrast, in the maladaptive RHF/PAH cohort, we observed a further significant decline in RV free wall capillaries and arterioles by 54% ($P < 0.01$) and 65% ($P < 0.001$), respectively, compared to the adaptive RV cohort (Figure 3B&C). No significant changes in vascularity were observed at 7- and 14-days post MCT administration.

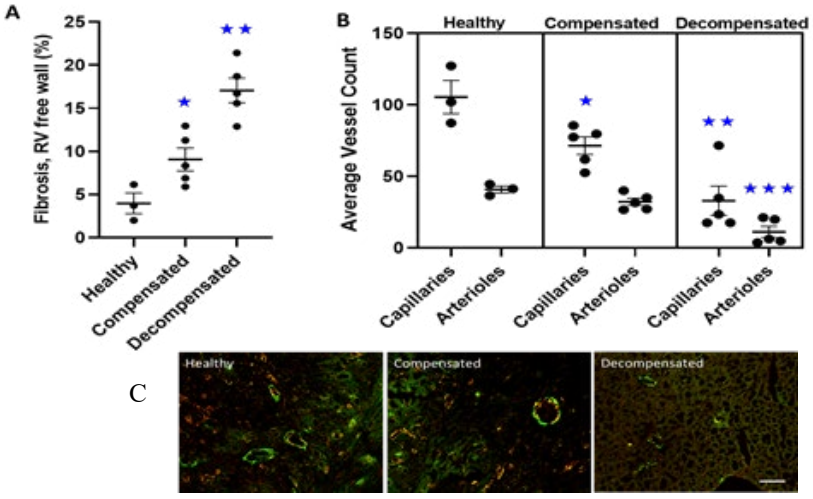

Figure 3A: The individual values and average percent fibrosis of the RV free wall in CTL, compensated and decompensated rat hearts is shown. *indicates significant difference from CTL ($P<0.05$). ** indicates significant difference from compensated hearts ($P<0.01$).

Figure 3B: Graphical representation of the average capillary and arteriole numbers per image for each animal is also demonstrated. *indicates significant difference from CTL ($P<0.05$). **indicates significant difference from compensated hearts ($P<0.05$). ***indicates significant difference from compensated hearts ($P<0.01$). Error bars indicate ± SEM.

Figure 3C: Example images of capillary (green) and arteriole density (orange) in different stages of PAH are shown. Scale bar = 50μm.

Hypertrophy-Related Gene Expression Changes in the RV Free Wall of Adapted and Maladapted PAH Animals

During the progression of PAH, the RV becomes progressively decompensated with the eventual development of overt RHF. Further, echocardiography data presented above, marked the transition of adaptive hypertrophy to maladaptive hypertrophy, however the molecular signaling that drives the maladaptation in PAH is unknown. While there is an abundance of literature on the signaling pathways associated with cardiac hypertrophy, those data predominantly reflect events in the LV. Measurements of gene expression related to hypertrophy in the RV is limited, especially for serial measures over time in the context of progression toward RHF. To gain insight into possible alterations in those signaling pathway patterns we described during the adaptive and maladaptive phases, we evaluated the IGF-1, MAPK/ERK, and mTOR pathways in the RV muscle of rats as PAH progresses.

IGF-1

IGF-1 is a potent regulator of inflammation and angiogenesis, and reduced IGF-1 has been described as part of the RV muscle failure molecular signature complicating PAH [30,31]. IGF-1 protein expression in the RV muscle of PAH rats were similar to that in CTL animals between days 7and 24 (Figure 4). At day 28 a significant 45% reduction ($P < 0.001$) in IGF-1 expression in the RV of PAH rats was noted compared to CTL (Figure 4). Right hearts undergoing maladaptive hypertrophy, at day 42, also showed a 45% decrease in IGF1.

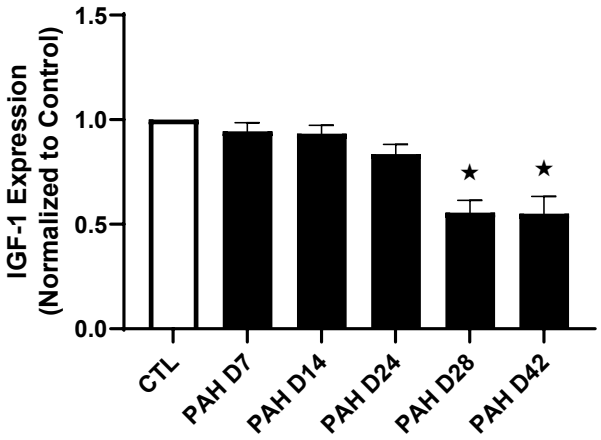

Figure 4: IGF-1 protein expression in the right ventricle (RV) of control (CTL) and pulmonary arterial hypertension (PAH) rats complicated by right heart failure (RHF), normalized to CTL expression values. ★Significantly different from CTL. Values are means ± SEM.

MAPK/ERK Pathway

Downstream of IGF-1 activation, the phosphorylation states of the signaling proteins p44 (ERK1) and p42 (ERK2) were both assessed. Values for both P-p44 and P-p42 were similar between CTL and PAH rats at days 7 and 14 (Figure 5). At day 24 however, significant increments were observed for both P-p44 (1.6-fold; $P < 0.001$) and P-p42 (1.4-fold; $P < 0.05$) in PAH rats compared to CTL. At day 28 P-p44 values were still 16% greater than CTL (NS), while P-p42 expression had returned to CTL values. In maladapted hearts, values for both P-p44 and P-p42 were similar between maladapted PAH and CTL rats (Figure 5).

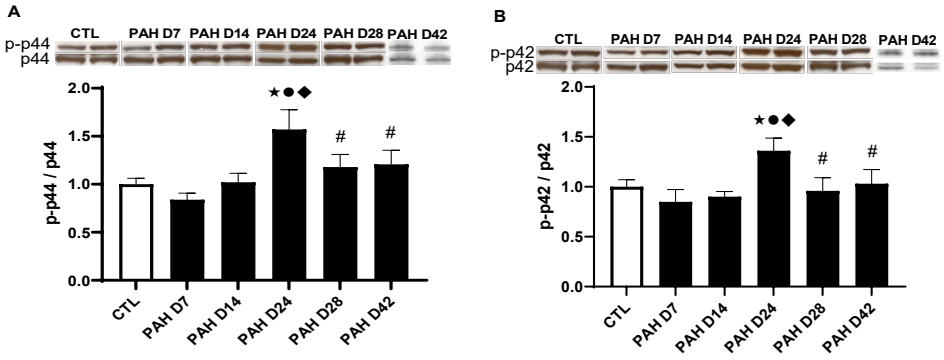

Figure 5A: P-p44 and

Figure 5B: P-p42 expression levels in the RV of control (CTL) and pulmonary arterial hypertension (PAH) rats complicated by right heart failure were expressed as a fraction of phosphorylated protein over total protein. Values are shown as means ± SEM.

GSK-3 Pathway

GSK-3β is known to play an important role in regulating glycogen metabolism in cardiac muscle and in the integration of hypertrophic signaling in the heart has been increasingly emphasized [17]. Phosphorylation of GSK-3B (Ser^9) inhibits its protein kinase activities, which diminishes GSK-3's inhibitory effects on eIF2 to promote protein translation and hypertrophy. Phospho-GSK-3β, values at days 7 and 14 were similar between CTL and PAH rats (Figure 6). However, P-GSK-3β was significantly increased by 1.3-fold in PAH rats at day 24 respectively ($P < 0.001$ and $P < 0.001$). At day 28, P-GSK-3β was significantly reduced ($P < 0.05$; Figure 6). Interestingly, there was no significant difference in phosphorylation of GSK-3β between maladapted/failed RV of PAH and CTL hearts.

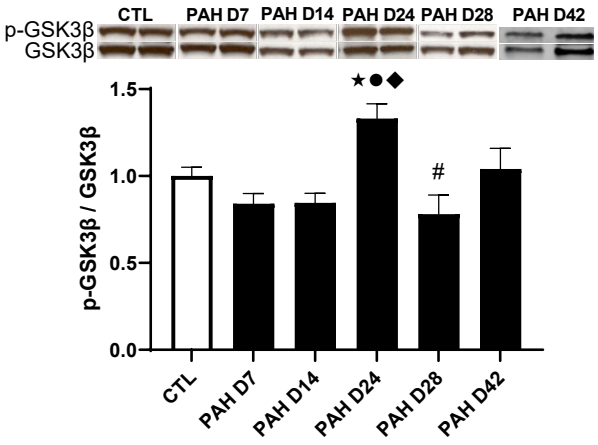

Figure 6: Values are means ± SEM; ★significantly different from CTL; •significantly different from day 7 PAH; •significantly different from day 14 PAH; # significantly different from day 24 PAH.

PI3K/Akt/mTOR Pathway

Levels of phosphorylated Akt, mTOR and down steam effectors, 4E-BP1 and p70^{S6K} were analyzed from RV cell lysates of healthy and PAH rats. P-Akt and P-mTOR were not significantly different between CTL and PAH rats at days 7 and 14. However, significant increments for both signaling proteins were observed at day 24 in PAH animals compared to CTL (1.3 and 1.4-fold increment respectively; $P < 0.05$ and $P < 0.01$; Figure 7A&B). At day 28, levels of P-Akt and P-mTOR had returned to control levels. Further out, phosphorylated Akt was diminished by 63% in the maladapted/failed RV muscle compared to control rats (Figure 7A; $P < 0.005$). P-mTOR, in maladaptive heart tissue, was significantly increased ($P < 0.01$; Figure 7B) suggesting activation by pathways separate from the PI3K/Akt signaling axis as P-Akt was markedly diminished.

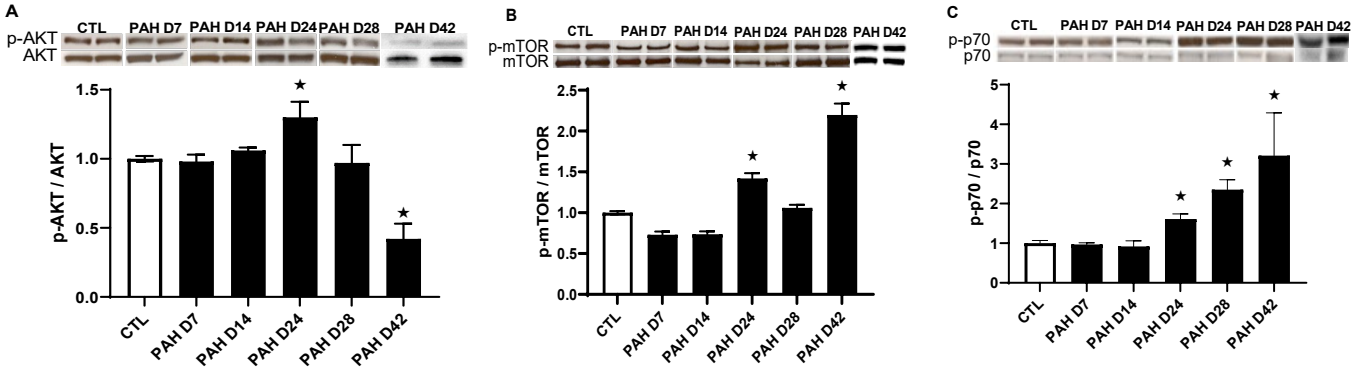

Figure 7A: Ratio of phosphorylated Akt (Ser^{473}) to total Akt,
Figure 7B: ratio of P-mTOR (Ser^{2448}) to total mTOR,
Figure 7C: p-p70^{S6K} (Thr^{389}) to total p70^{S6K} in the right ventricle of control (CTL) and pulmonary arterial hypertension (PAH) animals at days 0, 7, 14, 24, 28 and 42. Values are means ± SEM; ★significantly different from CTL.

The downstream effector P-p70^{S6K} was unchangedat days 7 and 14 in PAH rats, but significantly elevated at days 24 and 28 compared to CTL (1.6 and 2.4-fold increments respectively; $P < 0.01$ and $P < 0.001$. At day 42, P-p70^{S6K} remained significantly higher than control (3-fold higher; $P < 0.01$). To further explain this, we examined another possible signaling pathway that has recently been described to activate mTOR with subsequent autophagy inhibition [32].

Autophagy Pathway

To assess the role of autophagy signaling in the failing right heart, the LC3BII/I ratio was analyzed as a surrogate marker of autophagosome formation. There was a significant decrease in the LC3BII/I ratio in maladapted/failed RV of PAH rats compared to CTL rats ($P < 0.05$; Figure 8A&D). A recent publication identified a p27/CDK2 axis in the regulation of mTOR-dependent inhibition of autophagy during heart failure [32]. p27 was significantly decreased in maladapted/failed RV of PAH rats relative to CTL ($P < 0.05$; Figure 8A&B). However, p-CDK2 was not statistically different ($P = 0.22$) in PAH rats which likely reflects variances and power influences (Figure 8A&C).

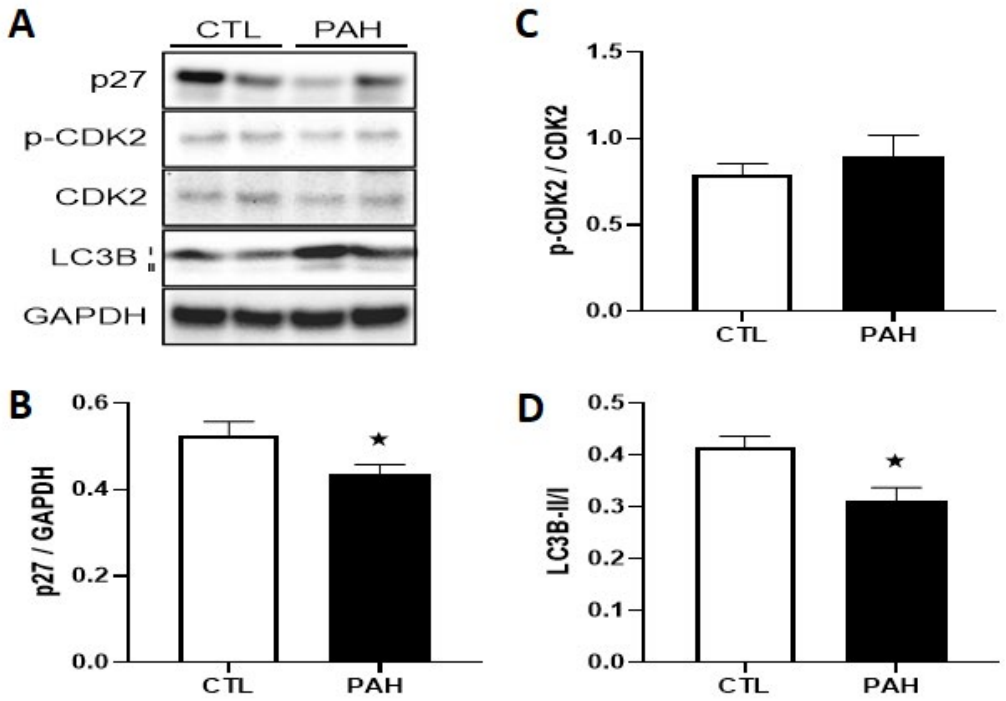

Figure 8A: Western blot analysis of autophagy marker expression in healthy and failing RV tissue. Graphical representations of protein levels.
Figure 8B: p27/GAPDH,
Figure 8C: phosphorylated p-CDK2/CDK2
Figure 8D: LCB3 I/II isoforms in the RV of control (CTL) and pulmonary arterial hypertension (PAH) rats complicated by right heart failure. ★Significantly different from CTL. Values are means±SEM. (F) Examples of Western Blots for each of the proteins described above.

Discussion

In this study, we evaluated over time, signaling events related to 3 key pathways known to be involved the early adaptive and physiologic response of the RV to the increased afterload presented to it in terms of in muscle protein synthesis and muscle hypertrophy in the adaptive phase of RV hypertrophy in the MCT model of PAH. We further examined in the phase of RV systolic decompensation/failure (often described as the maladaptive phase) what changes in these signaling pathways ensue and their consequences, particularly with prolonged mTOR activation [33]. What became evident is that even in the adaptive hypertrophy phase, there was the start of increased RV muscle fibrosis and a decline in RV muscle capillarity both of which markedly progressed further in the hemodynamically defined state of maladaptive hypertrophy.

RV Function and morphology

The time course studies revealed that a significant increase in RV systolic pressure predated the development of RV hypertrophy in PAH animals, like that described in previous studies [34,35]. Previously, we had demonstrated that RV systolic pressure was significantly increased in rats during the adaptive phase of PAH, while heart function, as measured by TAPSE and CO, was maintained at normative levels [34]. In maladaptive hearts, TAPSE and CO were significantly reduced. This suggests that pressure overload was an important early stimulus to RV hypertrophy in an adaptive fashion. Additionally, although the rats exhibited no clinical features of RV failure, there was evident a 2-fold increase in RV fibrosis compared with healthy controls and a 34% decrease in capillarity as depicted in Figure 3. This in part may not be that unexpected, as there are robust data that RV diastolic dysfunction is evident in animal models of PAH and which precedes RV systolic dysfunction. RV diastolic dysfunction, with associated RV wall stiffness, impaired filling and prolonged relaxation is felt to be associated with RV myocardial fibrosis [36-38]. The reduced capillarity in the adaptive phase is intriguing and suggests multiple impacts on angiogenesis even at this early stage. During the maladaptive phase, capillarity was reduced ~60% of healthy RV tissue while fibrosis had increased fourfold. Thus, a continuum of effects likely ensues in this progressive condition. Exactly what promotes the change is unknown. We speculate that when the burden of pathobiologic factors reaches a critical threshold, pathophysiologic features of RV systolic dysfunction and decompensation ensues.

Signaling Pathways

IGF-1

The IGF-1 data we report in this time series study of adaptive and maladaptive RV hypertrophy are intriguing. While we hypothesized the levels of IGF-1, a potential driver of hypertrophy, would increase in RV tissue as PAH progressed. However, no significant increment in IGF-1 expression was noted at any time point and at day 28 a significant 45% decrement was observed. Furthermore, maladaptive RVs expressed half the IGF-1 as the healthy controls. We speculate that several possible factors may have acted to impair translation of IGF-1 mRNA in our mod-

el. Firstly, inflammation has recently been highlighted in the pathobiology of PAH and most certainly plays a role in the MCT model [39-41]. Indeed, inflammatory cytokines such as tumor necrosis factor (TNF)-α can inhibit the action of IGF-1 in muscle [42]. Of interest, MCT -induced PAH in rats was attenuated by TNF-α antagonists via the suppression of TNF-α expression and the NF-κB pathway [43]. Further, MCT has been reported to activate NF-κB expression in the RV of the MCT-induced PAH model [44]. In addition, several inflammatory cytokines, including TNF-α, IL-1β and IL-6, are expressed in heart muscle and upregulated in heart failure and in the MCT model [45,46]. Thus IGF-1 expression may have been suppressed by the action of inflammatory cytokines. Significant body weight loss was observed in the PAH animals at days 24 and 28 compared with controls and malnutrition may also suppress IGF-1 expression in muscle tissue [29].

The significantly reduced levels of IGF-1 in maladaptive hearts suggest that many of the protean actions of IGF-1 on cardiac muscle would be severely impaired, such as its anabolic influences on RV muscle protein synthesis, as well as its anti-apoptotic, pro-angiogenic and positive inotropic actions, all of which could impair RV muscle function and contribute to the "sick" RV muscle milieu with RV decompensation and failure [47-50]. While we focused our studies on 3 major signaling pathways, we cannot rule out influences due to crosstalk with other pathways known to be implicated in cardiac muscle hypertrophy.

MAPK/ERK Pathway

The MAPK comprises several family subtypes and is ubiquitously expressed amongst the body tissues, including in cardiac muscle [51]. The ERK1/2 subfamily is a prototypical pathway mainly responsive to growth factors (e.g., IGF-1 and insulin), while the p38 and JNK subfamilies are more "stress" responsive [52]. Activation of ERK1/2 by IGF-1 can occur via its tyrosine kinase receptor or independently, possibly via G proteins [53]. The Ras/Raf/Mek/ERK1/2 signaling pathways are regarded as having significant influences in promoting cardio myocyte hypertrophy, in both in vitro as well as in vivo cardiac specific genetic models [18, 20]. While ERK1/2 activation has been described with left-sided pressure overload, there is a paucity of data on ERK pathways in the context of right-sided pressure overload and RV hypertrophy [54]. Increased levels of activated ERK were however reported in the RV in pulmonary artery banded fetal sheep [19]. It is thus of interest to report significantly increased expression of P-ERK1 and P-ERK2 at day 24 in PAH animals compared to controls, a time point at which significant RV hypertrophy emerged. Further, both P-ERK1/2 protein levels decreased to control levels at day 28 and maintained similar expression levels in maladapted hearts. In and of itself, it is unclear whether the ERK pathways are a dominant component of RV hypertrophy per se, or whether they only exert positive influences in conjunction with the effects of other signaling pathways [51].

GSK3 Pathway

As mentioned above, GSK-3 governs the regulation of glycogen metabolism and hypertrophy of cardiac muscle [17]. While inhibition of GSK-3 in cardiac myocytes can be mediated by several other kinases (see below), its inhibition is likely largely mediated via PI3K/Akt signaling, with IGF-1 (and insulin) the most potent activators of Akt [51]. In the present study, there was increased phosphorylation of GSK-3β, similar in time to increased ERK phosphorylation, which coincided in time with the onset of RV hypertrophy at day 24. Shortly after the spike in GSK-3β phosphorylation levels, P-GSK-3β expression return to healthy levels and remained at similar levels in maladaptive hearts. It is unclear what signal/s mediated this effect. In states of nutritional stress, we reported that GSK-3 and ERK expression was suppressed along with reduced p-Akt [15]. However, it is of interest that GSK-3β was previously reported as increased in the RV of MCT treated rats as well as in the LV of LV pressure overload and heart failure with a late reduction reported [55,56]. We speculate that the preservation of GSK-3 expression may reflect an attempt to preserve muscle protein synthesis in an otherwise stress-induced catabolic and apoptotic environment.

PI3K/Akt/ mTOR Pathway

In the present study, P-Akt, and P-mTOR were significantly upregulated at day 24 while the downstream effector, P-p70^{S6K} was significantly upregulated at days 24 and 28, suggesting signaling events likely to impact on cardiac muscle protein synthesis. Akt activation phosphorylates a key regulatory domain of mTOR, which acts on the downstream target, p70^{S6K}. Of note, p70^{S6K} phosphorylates a 40S ribosomal protein S6, resulting in enhanced ribosomal binding capacity and protein translation for essential components of the muscle protein synthesis apparatus. The PI3K/Akt/mTOR pathway has also been shown to be upregulated in several models of hypertrophy of the LV, including in response to pressure overload [e.g., 10-12]. In the decompensated /failed RV of PAH rats, a marked reduction in phosphorylated Akt was found. Similar findings have been reported in several animal models of the pressure overloaded LV accompanied by LV hypertrophy and heart failure due to transverse aortic constriction or with doxorubicin-induced cardiomyopathy [56-58]. The PI3K/Akt pathway has been highlighted as important in physiologic adaptive cardiac hypertrophy and to exert a protective role particularly under conditions of stress. Thus, the markedly diminished expression of p-Akt in the decompensated RV muscle would be expected to negatively impact on several signaling pathways known to promote a healthy RV milieu. Our findings are in contrast to those reported for the Sugen/Hypoxia model of PAH and RV decompensation in which mTORC2-Akt levels were unaffected, while mTORC1 signaling in the RV muscle was upregulated [14]. Unexpectedly, a significant and marked increase in p-mTOR expression was found in the maladapted RV muscle. Thus, it appears that mTOR is not activated via the PI3K/Akt pathway in maladaptive RV hypertrophy, unlike signaling in adaptive RV hypertrophy. Similarly, Deng and coworkers reported increased p-mTOR in the decompensated/ failed RV muscle 42 days post MCT administration in rats [59]. Further, Pena and coworkers reported upregulation of mTORC1 in the maladapted RV of rats with severe PAH induced by Sugen/Hypoxia [14]. We thus evaluated other possible sources of mTOR activation independent of Akt and ERK signaling, as described below.

Dysregulated Autophagy and Implications for Right Heart Failure

Recently a p27/cyclin dependent kinase inhibitor (CDK2)/mTOR signaling pathway has been described in cardiac muscle regulated by miR-221 [32]. Activation of this pathway has been shown to increase the expression and activity of mTOR. In cardio myocytes, p27 has been shown to be anti-hypertrophic and is down regulated in heart failure in response to pressure overload [60,61]. Moreover, mice deficient of p27 develop cardiac hypertrophy and heart failure [62]. What has also been observed in transgenic mice in which miR-221 (or miR-222) are overexpressed, is that there is the induction of heart failure with associated mTOR activation and autophagy inhibition [32, 63].

Autophagy is a conserved intracellular process geared to remove misfolded proteins and damaged intracellular organelles which are digested in autophagolysosomes [64]. Autophagy inhibition mediated by activated mTOR, transcription factor EB, miR-365 and Eva-1 homologue a knockout, are all associated with the development of heart failure [65-68]. Autophagy inhibition may also promote apoptosis of cardio myocytes [63].

In the present study, we demonstrated that p27 is significantly downregulated in the maladapted RV muscle and that mTOR is increased with evidence to suggest autophagy inhibition as evinced by significant decrease in the LC3BII/I ratio, suggesting this signaling axis is active in our model. Further it has been proposed that pronged mTORC1 activation in the RV muscle in the Sugen/Hypoxia model of PAH results in decreased autophagy [33].

Crosstalk between Signaling Pathways

The pathways leading to RV hypertrophy in our model of PAH are clearly complex and likely involve signals from multiple key pathways as well as interaction with or crosstalk between the varieties of signals elaborated in this model. The calcium-dependent phosphatase, calcineurin, for example, has been implicated in pathological models of LV hypertrophy. Calcineurin dephosphorylates the transcription factor, NFAT-3 (nuclear factor of activated Tcells-3), which in combination with another transcription factor, GATA4, synergistically promotes cardiac gene transcription and hypertrophy [69,70]. Of note, IGF-1 increases P-GATA4 and its nuclear accumulation in cardiac myocytes, while GSK-3β and ERK1/2 have also been shown to activate GATA4 in vitro [71-73]. However, GATA4 has robustly been shown not to be required for IGF-1 induced cardiac hypertrophy, which can proceed in its absence [71]. Further, activation of ERK1/2 by IGF-1 in cardio myocytes may in part be mediated by protein kinase C alpha (PKCα) [74]. In our model, P-p70^{S6K} was upregulated in the RV of PAH animals at days 24 and 28 likely mediated in large part by Akt/mTOR pathways. Interestingly, crosstalk between ERK and p70^{S6K} has been reported in cardio myocytes [75].

Apart from PI3K/Akt mediated phosphorylation and inhibition of GSK-3α and β, other signaling pathways have been demonstrated to also phosphorylate and inactivate GSK-3 acting upon the same inhibitory sites as Akt [17]. These include Gq protein coupled receptor (GqPCR) agonists such as endothelin-1 (ET-1), which is upregulated in PAH. ET-1 can stimulate PKC with subsequent activation of the ERK1/2 signaling cascade [16]. Further, ERK1/2 can phosphorylate and activate p90-ribosomal S6 kinase (RSK), which can then phosphorylate and inhibit GSK-3. Ligands for both α and β adrenoreceptors can phosphorylate GSK-3β, possibly via Akt activation [76]. Further, S6 kinases, Fas, and PKA can also inhibit GSK-3 [17].

Several pathways can signal through ERK to facilitate cardio myocyte hypertrophy. In addition to growth factor signaling via tyrosine kinase receptors, signaling by adrenergic agonists, angiotensin and ET-1 via GqPCRs can also occur via MEK/ERK pathway signaling to mediate cardiac muscle protein synthesis and hypertrophy [51,77].

Conclusions

This paper provides the most comprehensive analysis of key signaling pathways involved in muscle protein synthesis in both the adaptive and maladaptive phases in the right ventricle (RV) in a model of pulmonary hypertension (PH). Although much of the data is descriptive, it provides key insights upon which future studies could be planned using cause and effect methodologies. Further, we report for the first time, strong data/inference that impaired autophagy plays a role in the failing RV dysfunction (reported previously for the LV) and which adds to the pathobiology of the dysfunctional and failing RV in PH, in which therapeutic approaches to offset this may be contemplated. Lastly, we report important insights that 2 key pathobiologic aberrations (i.e. loss of RV capillarity and increase in RV muscle fibrosis), start in the adaptive phase and serially worsen in the maladaptive phase, which may have meaningful clinical implications for much earlier treatment measures directed at the RV muscle in patients with PH [78-82].

Abbreviations

PAH: Pulmonary Arterial Hypertension
RV: Right Ventricle
LV: Left Ventricle
S: Septum
RHF: Right Heart Failure
MCT: Monocrotaline
CTL: Control
TAPSE: Tricuspid Annular Systolic Plane Excursion
PA VTI: Pulmonary Artery Velocity Time Integral
SV: Stroke Volume
CO: Cardiac Output

Author Contributions

Conception/Design of Study: Mario Fournier and Michael I Lewis
Data Collection and Analysis: Mario Fournier, Russell G Rogers, Ryan C Middleton, Brandon S Grimes and Xuan Xu
Data Interpretation: Mario Fournier, Russell G Rogers, Ryan C Middleton and Michael I Lewis
Statistical Analysis and Figures: Mario Fournier, Ryan C Middleton, Russell G Rogers and Michael I Lewis
Drafting of Manuscript: Mario Fournier, Ryan C Middleton,

Brandon S Grimes and Michael I Lewis
Editing and Revising of Manuscript: Ryan C Middleton and Michael I Lewis
Final Version Approval: Michael I Lewis

Acknowledgements

The authors gratefully acknowledge Guangzhu Zhang for her skilled technical assistance and Eduardo Marbán, M.D., Ph.D., for his insightful review and advice on this project.

Availability of the data

The datasets used and/or analyzed during the current study will be made available from the corresponding author on reasonable request.

Declarations

Animal Welfare Ethics Approval

This research conformed to the Guide for the Care and Use of Laboratory Animals (NIH Publication No. 85–23, revised 1996). The research protocol was approved by the Institutional Animal Care and Use Committee of the Burns and Allen Research Institute at Cedars Sinai Medical Center.

Funding

This work was supported by research grants from the Brandman Foundation, the Plum Foundation and the California Institute of Regenerative Medicine (CLIN2-09444). These sponsors provided only financial support for the conduct of the research and had no involvement in any scientific aspect of the study.

References

1. Humbert, M., Sitbon, O., Chaouat, A., Bertocchi, M., Habib, G., Gressin, V., ... & Simonneau, G. (2010). Survival in patients with idiopathic, familial, and anorexigen-associated pulmonary arterial hypertension in the modern management era. Circulation, 122(2), 156-163.
2. Farber, H. W., Miller, D. P., Poms, A. D., Badesch, D. B., Frost, A. E., Muros-Le Rouzic, E., ... & Benza, R. L. (2015). Five-year outcomes of patients enrolled in the REVEAL Registry. Chest, 148(4), 1043-1054.
3. Barst, R. J., Chung, L., Zamanian, R. T., Turner, M., & McGoon, M. D. (2013). Functional class improvement and 3-year survival outcomes in patients with pulmonary arterial hypertension in the REVEAL Registry. Chest, 144(1), 160-168.
4. Vonk-Noordegraaf, A., Haddad, F., Chin, K. M., Forfia, P. R., Kawut, S. M., Lumens, J., ... & Hassoun, P. M. (2013). Right heart adaptation to pulmonary arterial hypertension: physiology and pathobiology. Journal of the American College of Cardiology, 62(25S), D22-D33.
5. Benza, R. L., Miller, D. P., Gomberg-Maitland, M., Frantz, R. P., Foreman, A. J., Coffey, C. S., ... & McGoon, M. D. (2010). Predicting survival in pulmonary arterial hypertension: insights from the registry to evaluate early and long-term pulmonary arterial hypertension disease management (REVEAL). Circulation, 122(2), 164-172.
6. Forfia, P. R., Fisher, M. R., Mathai, S. C., Housten-Harris, T., Hemnes, A. R., Borlaug, B. A., ... & Hassoun, P. M. (2006). Tricuspid annular displacement predicts survival in pulmonary hypertension. American journal of respiratory and critical care medicine, 174(9), 1034-1041.
7. Mauritz, G. J., Kind, T., Marcus, J. T., Bogaard, H. J., van de Veerdonk, M., Postmus, P. E., ... & Vonk-Noordegraaf, A. (2012). Progressive changes in right ventricular geometric shortening and long-term survival in pulmonary arterial hypertension. Chest, 141(4), 935-943.
8. D'Alonzo, G. E., Barst, R. J., Ayres, S. M., Bergofsky, E. H., Brundage, B. H., Detre, K. M., ... & Wu, M. (1991). Survival in patients with primary pulmonary hypertension: results from a national prospective registry. Annals of internal medicine, 115(5), 343-349.
9. Bodine, S. C., Stitt, T. N., Gonzalez, M., Kline, W. O., Stover, G. L., Bauerlein, R., ... & Yancopoulos, G. D. (2001). Akt/mTOR pathway is a crucial regulator of skeletal muscle hypertrophy and can prevent muscle atrophy in vivo. Nature cell biology, 3(11), 1014-1019.
10. Hua, Y., Zhang, Y., & Ren, J. (2012). IGF-1 deficiency resists cardiac hypertrophy and myocardial contractile dysfunction: role of microRNA-1 and microRNA-133a. Journal of cellular and molecular medicine, 16(1), 83-95.
11. Kim, J., Wende, A. R., Sena, S., Theobald, H. A., Soto, J., Sloan, C., ... & Abel, E. D. (2008). Insulin-like growth factor I receptor signaling is required for exercise-induced cardiac hypertrophy. Molecular endocrinology, 22(11), 2531-2543.
12. McMullen, J. R., Shioi, T., Huang, W. Y., Zhang, L., Tarnavski, O., Bisping, E., ... & Izumo, S. (2004). The insulin-like growth factor 1 receptor induces physiological heart growth via the phosphoinositide 3-kinase (p110α) pathway. Journal of Biological Chemistry, 279(6), 4782-4793.
13. Vary, T. C., & Lang, C. H. (2005). IGF-I activates the eIF4F system in cardiac muscle in vivo. Molecular and cellular biochemistry, 272(1), 209-220.
14. Pena, A., Kobir, A., Goncharov, D., Goda, A., Kudryashova, T. V., Ray, A., ... & Goncharova, E. A. (2017). Pharmacological inhibition of mTOR kinase reverses right ventricle remodeling and improves right ventricle structure and function in rats. American journal of respiratory cell and molecular biology, 57(5), 615-625.
15. Lewis, M. I., Bodine, S. C., Kamangar, N., Xu, X., Da, X., & Fournier, M. (2006). Effect of severe short-term malnutrition on diaphragm muscle signal transduction pathways influencing protein turnover. Journal of Applied Physiology, 100(6), 1799-1806.
16. Markou, T., Cullingford, T. E., Giraldo, A., Weiss, S. C., Alsafi, A., Fuller, S. J., ... & Sugden, P. H. (2008). Glycogen synthase kinases 3α and 3β in cardiac myocytes: regulation and consequences of their inhibition. Cellular signalling, 20(1), 206-218.
17. Sugden, P. H., Fuller, S. J., Weiss, S. C., & Clerk, A. (2008). Glycogen synthase kinase 3 (GSK3) in the heart: a point of integration in hypertrophic signalling and a therapeutic target? A critical analysis. British journal of pharmacology, 153(S1), S137-S153.
18. Bueno, O. F., De Windt, L. J., Tymitz, K. M., Witt, S. A., Kimball, T. R., Klevitsky, R., ... & Molkentin, J. D. (2000). The MEK1–ERK1/2 signaling pathway promotes compen-

sated cardiac hypertrophy in transgenic mice. The EMBO journal, 19(23), 6341-6350.
19. Olson, A. K., Protheroe, K. N., Scholz, T. D., & Segar, J. L. (2008). Activation of the mitogen-activated protein kinases and Akt in response to pulmonary artery banding in the fetal sheep heart is developmentally regulated. Neonatology, 93(3), 145-152.
20. Ueyama, T., Kawashima, S., Sakoda, T., Rikitake, Y., Ishida, T., Kawai, M., ... & Yokoyama, M. (2000). Requirement of activation of the extracellular signal-regulated kinase cascade in myocardial cell hypertrophy. Journal of molecular and cellular cardiology, 32(6), 947-960.
21. Lewis, M. I., Horvitz, G. D., Clemmons, D. R., & Fournier, M. (2002). Role of IGF-I and IGF-binding proteins within diaphragm muscle in modulating the effects of nandrolone. American Journal of Physiology-Endocrinology and Metabolism, 282(2), E483-E490.
22. Ebensperger, R., Acevedo, E., Meléndez, J., Corbalán, R., Acevedo, M., Sapag-Hagar, M., ... & Lavandero, S. (1998). Selective increase in cardiac IGF-1 in a rat model of ventricular hypertrophy. Biochemical and biophysical research communications, 243(1), 20-24.
23. Honsho, S., Nishikawa, S., Amano, K., Zen, K., Adachi, Y., Kishita, E., ... & Matsubara, H. (2009). Pressure-mediated hypertrophy and mechanical stretch induces IL-1 release and subsequent IGF-1 generation to maintain compensative hypertrophy by affecting Akt and JNK pathways. Circulation research, 105(11), 1149-1158.
24. McMullen, J. R., Shioi, T., Zhang, L., Tarnavski, O., Sherwood, M. C., Kang, P. M., & Izumo, S. (2003). Phosphoinositide 3-kinase (p110α) plays a critical role for the induction of physiological, but not pathological, cardiac hypertrophy. Proceedings of the National Academy of Sciences, 100(21), 12355-12360.
25. http://www.ihcworld.com/_protocols/special_stains/sirius_red.htm
26. Whittaker, P., Kloner, R. A., Boughner, D. R., & Pickering, J. G. (1994). Quantitative assessment of myocardial collagen with picrosirius red staining and circularly polarized light. Basic research in cardiology, 89(5), 397-410.
27. Hadi, A. M., Mouchaers, K. T., Schalij, I., Grunberg, K., Meijer, G. A., Vonk-Noordegraaf, A., ... & Beliën, J. A. (2010). Rapid quantification of myocardial fibrosis: a new macro-based automated analysis. Analytical Cellular Pathology, 33(5-6), 257-269.
28. https://imagej.nih.gov/ij/docs/examples/stained-sections/index.html
29. Lewis, M. I., Li, H., Huang, Z. S., Biring, M. S., Cercek, B., & Fournier, M. (2003). Influence of varying degrees of malnutrition on IGF-I expression in the rat diaphragm. Journal of Applied Physiology, 95(2), 555-562.
30. Bach, L. A. (2015). Endothelial cells and the IGF system. J Mol Endocrinol, 54(1), R1-R13.
31. Drake, J. I., Bogaard, H. J., Mizuno, S., Clifton, B., Xie, B., Gao, Y., ... & Natarajan, R. (2011). Molecular signature of a right heart failure program in chronic severe pulmonary hypertension. American journal of respiratory cell and molecular biology, 45(6), 1239-1247.
32. Su, M., Wang, J., Wang, C., Wang, X., Dong, W., Qiu, W., ... & Hui, R. (2015). MicroRNA-221 inhibits autophagy and promotes heart failure by modulating the p27/CDK2/mTOR axis. Cell Death & Differentiation, 22(6), 986-999.
33. Houssaini, A., & Adnot, S. (2017). mTOR: a key to both pulmonary vessel remodeling and right ventricular function in pulmonary arterial hypertension?. American Journal of Respiratory Cell and Molecular Biology, 57(5), 509-511.
34. Middleton, R. C., Fournier, M., Xu, X., Marbán, E., & Lewis, M. I. (2017). Therapeutic benefits of intravenous cardiosphere-derived cell therapy in rats with pulmonary hypertension. PLoS One, 12(8), e0183557.
35. Henkens, I. R., Mouchaers, K. T., Vliegen, H. W., van der Laarse, W. J., Swenne, C. A.,.....& Vonk-Noordegraaf, A. (2007). Early changes in rat hearts with developing pulmonary arterial hypertension can be detected with three-dimensional electrocardiography. Am J Physiol Heart Circ Physiol, 293, H1300-H1307.
36. Rain, S., Handoko, M. L., Trip, P., Gan, C. T. J., Westerhof, N., Stienen, G. J., ... & de Man, F. S. (2013). Right ventricular diastolic impairment in patients with pulmonary arterial hypertension. Circulation, 128(18), 2016-2025.
37. Trip, P., Rain, S., Handoko, M. L., Van der Bruggen, C., Bogaard, H. J., Marcus, J. T., ... & Frances, S. (2015). Clinical relevance of right ventricular diastolic stiffness in pulmonary hypertension. European Respiratory Journal, 45(6), 1603-1612.
38. Murch, S. D., Gerche, A. L., Roberts, T. J., Prior, D. L., MacIsaac, A. I., & Burns, A. T. (2015). Abnormal right ventricular relaxation in pulmonary hypertension. Pulmonary circulation, 5(2), 370-375.
39. Wilson, D. W., Segall, H. J., Pan, L. C., & Dunston, S. K. (1989). Progressive inflammatory and structural changes in the pulmonary vasculature of monocrotaline-treated rats. Microvascular research, 38(1), 57-80.
40. Rabinovitch, M., Guignabert, C., Humbert, M., & Nicolls, M. R. (2014). Inflammation and immunity in the pathogenesis of pulmonary arterial hypertension. Circulation research, 115(1), 165-175.
41. Le Hiress, M., Tu, L., Ricard, N., Phan, C., Thuillet, R., Fadel, E., ... & Guignabert, C. (2015). Proinflammatory signature of the dysfunctional endothelium in pulmonary hypertension. Role of the macrophage migration inhibitory factor/CD74 complex. American journal of respiratory and critical care medicine, 192(8), 983-997.
42. Fernández-Celemín, L., Pasko, N., Blomart, V., & Thissen, J. P. (2002). Inhibition of muscle insulin-like growth factor I expression by tumor necrosis factor-α. American Journal of Physiology-Endocrinology and Metabolism, 283(6), E1279-E1290.
43. Wang, Q., Zuo, X. R., Wang, Y. Y., Xie, W. P., Wang, H., & Zhang, M. (2013). Monocrotaline-induced pulmonary arterial hypertension is attenuated by TNF-α antagonists via the suppression of TNF-α expression and NF-κB pathway in rats. Vascular pharmacology, 58(1-2), 71-77.
44. Kumar, S., Wei, C., Thomas, C. M., Kim, I. K., Seqqat, R., Kumar, R., ... & Gupta, S. (2012). Cardiac-specific genetic inhibition of nuclear factor-κB prevents right ventricular

hypertrophy induced by monocrotaline. American Journal of Physiology-Heart and Circulatory Physiology, 302(8), H1655-H1666.
45. Price, L. C., Montani, D., Tcherakian, C., Dorfmüller, P., Souza, R., Gambaryan, N., ... & Perros, F. (2011). Dexamethasone reverses monocrotaline-induced pulmonary arterial hypertension in rats. European Respiratory Journal, 37(4), 813-822.
46. Kubota, T., Miyagishima, M., Alvarez Jr, R. J., Kormos, R., Rosenblum, W. D., Demetris, A. J., ... & McNamara, D. M. (2000). Expression of proinflammatory cytokines in the failing human heart: comparison of recent-onset and end-stage congestive heart failure. The Journal of heart and lung transplantation, 19(9), 819-824.
47. van de Veerdonk, M. C., Bogaard, H. J., & Voelkel, N. F. (2016). The right ventricle and pulmonary hypertension. Heart failure reviews, 21(3), 259-271.
48. Reddy, S., & Bernstein, D. (2015). Molecular mechanisms of right ventricular failure. Circulation, 132(18), 1734-1742.
49. Ryan, J. J., Huston, J., Kutty, S., Hatton, N. D., Bowman, L., Tian, L., ... & Archer, S. L. (2015). Right ventricular adaptation and failure in pulmonary arterial hypertension. Canadian Journal of Cardiology, 31(4), 391-406.
50. Bogaard, H. J., Abe, K., Noordegraaf, A. V., & Voelkel, N. F. (2009). The right ventricle under pressure: cellular and molecular mechanisms of right-heart failure in pulmonary hypertension. Chest, 135(3), 794-804.
51. Rose, B. A., Force, T., & Wang, Y. (2010). Mitogen-activated protein kinase signaling in the heart: angels versus demons in a heart-breaking tale. Physiological reviews, 90(4), 1507-1546.
52. Ramos, J. W. (2008). The regulation of extracellular signal-regulated kinase (ERK) in mammalian cells. The international journal of biochemistry & cell biology, 40(12), 2707-2719.
53. Perrault, R., Wright, B., Storie, B., Hatherell, A., & Zahradka, P. (2011). Tyrosine kinase-independent activation of extracellular-regulated kinase (ERK) 1/2 by the insulin-like growth factor-1 receptor. Cellular signalling, 23(4), 739-746.
54. Takeishi, Y., Huang, Q., Abe, J. I., Glassman, M., Che, W., Lee, J. D., ... & Walsh, R. A. (2001). Src and multiple MAP kinase activation in cardiac hypertrophy and congestive heart failure under chronic pressure-overload: comparison with acute mechanical stretch. Journal of molecular and cellular cardiology, 33(9), 1637-1648.
55. Colombo, R., Siqueira, R., Becker, C. U., Fernandes, T. G., Pires, K. M., Valença, S. S., ... & Belló-Klein, A. (2013). Effects of exercise on monocrotaline-induced changes in right heart function and pulmonary artery remodeling in rats. Canadian journal of physiology and pharmacology, 91(1), 38-44.
56. Li, X. M., Ma, Y. T., Yang, Y. N., Liu, F., Chen, B. D., Han, W., ... & Gao, X. M. (2009). Downregulation of survival signalling pathways and increased apoptosis in the transition of pressure overload-induced cardiac hypertrophy to heart failure. Clinical and Experimental Pharmacology and Physiology, 36(11), 1054-1061.
57. Kemi, O. J., Ceci, M., Wisloff, U., Grimaldi, S., Gallo, P., Smith, G. L., ... & Ellingsen, O. (2008). Activation or inactivation of cardiac Akt/mTOR signaling diverges physiological from pathological hypertrophy. Journal of cellular physiology, 214(2), 316-321.
58. Chen, Y. L., Chung, S. Y., Chai, H. T., Chen, C. H., Liu, C. F., Chen, Y. L., ... & Yip, H. K. (2015). Early administration of carvedilol protected against doxorubicin-induced cardiomyopathy. Journal of Pharmacology and Experimental Therapeutics, 355(3), 516-527.
59. Deng, Y., Wu, W., Guo, S., Chen, Y., Liu, C., Gao, X., & Wei, B. (2017). Altered mTOR and Beclin-1 mediated autophagic activation during right ventricular remodeling in monocrotaline-induced pulmonary hypertension. Respiratory research, 18(1), 1-15.
60. Li, J. M., & Brooks, G. A. V. I. N. (1997). Downregulation of cyclin-dependent kinase inhibitors p21 and p27 in pressure-overload hypertrophy. American Journal of Physiology-Heart and Circulatory Physiology, 273(3), H1358-H1367.
61. Burton, P. B., Yacoub, M. H., Barton, P. J. (1999).Cyclin-dependent kinase inhibitor expression in human heart failure. A comparison with fetal development. Eur Heart J, 20, 604-611.
62. Hauck, L., Harms, C., An, J., Rohne, J., Gertz, K., Dietz, R., ... & von Harsdorf, R. (2008). Protein kinase CK2 links extracellular growth factor signaling with the control of p27Kip1 stability in the heart. Nature medicine, 14(3), 315-324.
63. Su, M., Chen, Z., Wang, C., Song, L., Zou, Y., Zhang, L., ... & Wang, J. (2016). Cardiac-specific overexpression of miR-222 induces heart failure and inhibits autophagy in mice. Cellular Physiology and Biochemistry, 39(4), 1503-1511.
64. Linton, P. J., Gurney, M., Sengstock, D., Mentzer Jr, R. M., & Gottlieb, R. A. (2015). This old heart: Cardiac aging and autophagy. Journal of molecular and cellular cardiology, 83, 44-54.
65. Bartlett, J. J., Trivedi, P. C., Yeung, P., Kienesberger, P. C., & Pulinilkunnil, T. (2016). Doxorubicin impairs cardiomyocyte viability by suppressing transcription factor EB expression and disrupting autophagy. Biochemical Journal, 473(21), 3769-3789.
66. Wu, H., Wang, Y., Wang, X., Li, R., & Yin, D. (2017). MicroRNA-365 accelerates cardiac hypertrophy by inhibiting autophagy via the modulation of Skp2 expression. Biochemical and biophysical research communications, 484(2), 304-310.
67. Zhang, S., Lin, X., Li, G., Shen, X., Niu, D., Lu, G., ... & Bai, Y. (2017). Knockout of Eva1a leads to rapid development of heart failure by impairing autophagy. Cell death & disease, 8(2), e2586-e2586.
68. Sciarretta, S., Forte, M., Frati, G., & Sadoshima, J. (2018). New insights into the role of mTOR signaling in the cardiovascular system. Circulation research, 122(3), 489-505.
69. Molkentin, J. D., Lu, J. R., Antos, C. L., Markham, B., Richardson, J., Robbins, J., ... & Olson, E. N. (1998). A calcineurin-dependent transcriptional pathway for cardiac hypertrophy. Cell, 93(2), 215-228.

70. Wilkins, B. J., Dai, Y. S., Bueno, O. F., Parsons, S. A., Xu, J., Plank, D. M., ... & Molkentin, J. D. (2004). Calcineurin/NFAT coupling participates in pathological, but not physiological, cardiac hypertrophy. Circulation research, 94(1), 110-118.
71. Bisping, E., Ikeda, S., Sedej, M., Wakula, P., McMullen, J. R., Tarnavski, O., ... & Pieske, B. (2012). Transcription factor GATA4 is activated but not required for insulin-like growth factor 1 (IGF1)-induced cardiac hypertrophy. Journal of Biological Chemistry, 287(13), 9827-9834.
72. Liang, Q., Wiese, R. J., Bueno, O. F., Dai, Y. S., Markham, B. E., & Molkentin, J. D. (2001). The transcription factor GATA4 is activated by extracellular signal-regulated kinase 1-and 2-mediated phosphorylation of serine 105 in cardiomyocytes. Molecular and cellular biology, 21(21), 7460-7469.
73. Morisco, C., Seta, K., Hardt, S. E., Lee, Y., Vatner, S. F., & Sadoshima, J. (2001). Glycogen synthase kinase 3β regulates GATA4 in cardiac myocytes. Journal of Biological Chemistry, 276(30), 28586-28597.
74. Pecherskaya, A., & Solem, M. (2000). IGF1 activates PKC α-dependent protein synthesis in adult rat cardiomyocytes. Molecular Cell Biology Research Communications, 4(3), 166-171.
75. Wang, L., Gout, I., & Proud, C. G. (2001). Cross-talk between the ERK and p70 S6 kinase (S6K) signaling pathways: MEK-dependent activation of S6K2 in cardiomyocytes. Journal of Biological Chemistry, 276(35), 32670-32677.
76. Morisco, C., Zebrowski, D., Condorelli, G., Tsichlis, P., Vatner, S. F., & Sadoshima, J. (2000). The Akt-glycogen synthase kinase 3β pathway regulates transcription of atrial natriuretic factor induced by β-adrenergic receptor stimulation in cardiac myocytes. Journal of Biological Chemistry, 275(19), 14466-14475.
77. Proud, C. G. (2004). Ras, PI3-kinase and mTOR signaling in cardiac hypertrophy. Cardiovascular research, 63(3), 403-413.
78. Vogel, J. (1997). Measurement of cardiac output in small laboratory animals using recordings of blood conductivity. American Journal of Physiology-Heart and Circulatory Physiology, 273(5), H2520-H2527.
79. Bartel, D. P. (2009). MicroRNAs: target recognition and regulatory functions. cell, 136(2), 215-233.
80. Elia, L., Contu, R., Quintavalle, M., Varrone, F., Chimenti, C., Russo, M. A., ... & Condorelli, G. (2009). Reciprocal regulation of microRNA-1 and insulin-like growth factor-1 signal transduction cascade in cardiac and skeletal muscle in physiological and pathological conditions. Circulation, 120(23), 2377-2385.
81. Hitachi, K., & Tsuchida, K. (2014). Role of microRNAs in skeletal muscle hypertrophy. Frontiers in physiology, 4, 408.
82. Purcell, N. H., Wilkins, B. J., York, A., Saba-El-Leil, M. K., Meloche, S., Robbins, J., & Molkentin, J. D. (2007). Genetic inhibition of cardiac ERK1/2 promotes stress-induced apoptosis and heart failure but has no effect on hypertrophy in vivo. Proceedings of the National Academy of Sciences, 104(35), 14074-14079.